Journal of Seismology **4:** 267–284, 2000.

A simple source inversion scheme for displacement seismograms recorded at short distances

S.K. Singh[1], M. Ordaz[2], J.F. Pacheco[1] & F. Courboulex[3]
[1]*Instituto de Geofísica, Universidad Nacional Autonoma de México, C.U., 041510 México D.F., Mexico;* [2]*Instituto de Ingeniería, Universidad Nacional Autonoma de México, C.U., 041510 México D.F., Mexico;* [3]*UMR, Géosciences Azur, 250 rue Albert Einstein, Sophia Antipolis, 06560 Valbonne, France*

Received 6 November 1998; accepted in revised form 1 July 1999

Key words: infinite-space synthetics, inversion of near-source data, near-field seismograms

Abstract

We have implemented and tested a simple inversion scheme to retrieve source parameters of small and moderate earthquakes recorded at close distances. The inversion assumes that such events may be approximated by a point-source shear dislocation, and the medium may be considered an infinite space. Theoretical seismograms used in the inversion include near- and intermediate-field contributions. The effect of free surface is approximately taken into account by multiplying the infinite-space synthetics by two. The location of the event is assumed to be known. Based on an examination of the data, the user chooses the length of the record and the weight of each trace to be used in the inversion. The shape of the source-time function is estimated from the observed seismograms. A grid search is performed to determine the focal mechanism and the seismic moment which minimizes the error between the observed and the synthetic seismograms. For two or more recordings, the inversion gives a solution which is consistent with the first-motion data and/or the moment tensor inversion of regional seismic waves. If only a single three-component recording is available then the inversion yields more than one equally acceptable focal mechanisms. In such cases, the first-motion polarities or a prior knowledge of the tectonics of the region is essential to constrain the solution. The test of the method on near-source broadband recordings of small and moderate earthquakes in Mexico and the aftershock sequence of 1997 Umbria-Marche, Italy shows that it gives fast, and surprisingly robust and reliable estimation of source parameters.

Introduction

High-quality, on-scale recordings of earthquakes at short distances from the source are now quite common. The displacement seismograms of these events are often simple and show contribution from near- and intermediate-field terms predicted by the theory (e.g., Kanamori et al., 1990; Ma and Kanamori, 1991, 1994; Romanowicz et al., 1993; Singh et al., 1997). These seismograms suggest that an infinite-space solution may be adequate to model them and, thereby, to extract source parameters. Since seismic waves at short distances from the source are less affected by path effect, it is clearly advantageous to utilize such recordings to infer source parameters. In this paper, we show that in many cases the Green's function of a point-source, shear-dislocation in an infinite space can, indeed, be fruitfully employed to invert recordings of small and moderate earthquakes at short distances.

The near-field elastodynamic solution of a point source in infinite space was obtained by G.G. Stokes about 150 years ago (Stokes, 1849). This solution is given in Love (1944, p. 305). Aki and Richards (1980, p. 81), and Ben-Menahem and Singh (1981, p. 220) give the solution for a point-source, shear dislocation, recasting it in a coordinate system appropriate for earthquake source studies. These authors also discuss the general characteristics of the solution. Wu and Ben-Menahem (1985, see also the references therein) have analyzed in detail the nature of the near-field solution. Aki (1968) and Anderson and Richards

(1975) have numerically integrated the point source Green's function to obtain near-field solution for different rupture scenarios on a finite fault. Recently, the near-field contribution from large and great earthquakes have been reported in seismograms recorded at regional and teleseismic distances (e.g., Vidale et al., 1995; Jiao et al., 1995).

Clearly, a layered, half space is a more realistic model to interpret near-source and regional seismograms. However, the computation of Green's functions for such models is cumbersome and time consuming. It also requires knowledge of the crustal structure which may be vary azimuthally. Sometimes, to speed up the analysis, the Green's functions corresponding to the three fundamental faults are computed previously and stored in a computer (see, e.g., Scrivner and Helmberger, 1995). A half-space model has also been successfully used in inverting local broadband recordings by taking advantage of the near- and intermediate-field contributions which is manifested by a ramp-like signal between P and S waves (see, e.g., Uhrhammer, 1992). In the Appendix we show that in the routine source inversion it may be preferable to discard complex SV waves and use an approximate half-space synthetics (i.e., infinite–space synthetics multiplied by two).This is so since, a priori, there is no reason to expect that the complexity of observed SV waves can be fit by half-space synthetic seismograms.

For near-source recordings, a point-source, shear dislocation in an infinite space may be an adequate approximation, provided that the source dimension is smaller than the distance to the station. If so, the analysis becomes very simple since the computation of Green's functions is elementary and fast. In this paper, we test this approach on near-source seismograms recorded in Mexico and in Italy. Ma and Kanamori (1991, 1994) have previously used infinite-space synthetics to analyze broadband seismograms recorded at close distances. They inverted amplitudes and polarities of P and SV waves on vertical component and SH wave on transverse component, using infinite-space far-field solution in the Green's function. Our synthetics include far-field as well as near- and intermediate-field terms. Furthermore, our inversion utilizes the waveforms, not just the peak amplitudes and their polarities.

A point source in an infinite space

We adopt the convention given in Aki and Richards (1980, Figures 4.13 and 4.20, p.114). Following Aki and Richards (1980, p. 81 and 115) and Ben-Menahem and Singh (1980, p. 200, 220, and 221) the displacement components in spherical coordinates, due to a point-source, shear dislocation of seismic moment M_0 located in an infinite space, can be written as

$$u^R = \frac{M_0}{4\pi\rho} F^R \Big[\frac{1}{R\alpha^3} \dot{g}(t - r/\alpha) + \frac{9}{R^4} \int_{R/\alpha}^{R/\beta} \tau g(t-\tau) d\tau + \frac{4}{R^2\alpha^2} g(t - R/\alpha) - \frac{3}{R^2\beta^2} g(t - R/\beta) \Big]$$

$$u^\theta = \frac{M_0}{4\pi\rho} F^\theta \Big[\frac{1}{R\beta^3} \dot{g}(t - r/\beta) - \frac{6}{R^4} \int_{R/\alpha}^{R/\beta} \tau g(t-\tau) d\tau - \frac{2}{R^2\alpha^2} g(t - R/\alpha) + \frac{3}{R^2\beta^2} g(t - R/\beta) \Big]$$

$$u^\varphi = \frac{M_0}{4\pi\rho} F^\varphi \Big[\frac{1}{R\beta^3} \dot{g}(t - r/\beta) - \frac{6}{R^4} \int_{R/\alpha}^{R/\beta} \tau g(t-\tau) d\tau - \frac{2}{R^2\alpha^2} g(t - R/\alpha) + \frac{3}{R^2\beta^2} g(t - R/\beta) \Big]$$

where $M_0\dot{g}(t)$ is the source-time function, so that $M_0 \int_0^\infty \dot{g}(t)dt = M_0$. In the equations above, R is the focal distance, α and β are the P and S-wave speeds, respectively, and ρ is the density. The first term in the square brackets is the far-field term, the second one is the near-field term, and the last two terms correspond to the intermediate-field terms. Below we will call the last three terms, collectively, as the near-field term. F^R, F^θ, and F^φ are the radiation pattern coefficients given by (Aki and Richards, 1980, p. 115):

$$\begin{aligned} \mathrm{F}^R = {} & \cos\lambda \sin\delta \sin^2 i_\xi \sin 2(\varphi - \varphi) \\ & - \cos\lambda \cos\delta \sin 2i_\xi \cos(\varphi - \varphi_s) + \\ & + \sin\lambda \sin 2\delta (\cos^2 i_\xi - \sin^2 i_\xi (\varphi - \varphi_s)) + \\ & + \sin\lambda \cos 2\delta \sin 2i_\xi \sin(\varphi - \varphi_s) \end{aligned}$$

$$\begin{aligned} \mathrm{F}^\theta = {} & \sin\lambda \cos 2\delta \cos 2 i_\xi \sin 2(\varphi - \varphi) \\ & - \cos\lambda \cos\delta \cos 2i_\xi \cos(\varphi - \varphi_s) + \\ & + \tfrac{1}{2} \cos\lambda \sin\delta \sin 2i_\xi \sin 2(\varphi - \varphi_s) - \\ & - \tfrac{1}{2} \sin\lambda \sin 2\delta \sin 2i_\xi (1 + \sin^2(\varphi - \varphi_s)) \end{aligned}$$

$$F^{\varphi} = \cos\lambda \cos\delta \cos i_{\xi} \sin(\varphi - \varphi) + \cos\lambda \sin\delta \sin i_{\xi} \cos 2(\varphi - \varphi_s) + \sin\lambda \cos 2\delta \cos i_{\xi} \cos(\varphi - \varphi_s) - \tfrac{1}{2} \sin\lambda \sin 2\delta \sin i_{\xi} \sin 2(\varphi - \varphi_s)$$

where φ, δ, and λ are azimuth, dip, and rake of the fault, φ_s is the azimuth of the station, and i_ξ is the take-off angle of the departing ray (see Aki and Richards, 1980, Fig. 4.20).

The displacement components, expressed in spherical coordinates above, can easily be transformed to any other desired orthogonal coordinate system, such as NS-EW-Z or radial-transverse-Z, to match the coordinate system of the data. Let the observed displacements in this system be U_{1j}, U_{2j}, U_{3j}, where j stands for station number. For a given focal mechanism and seismic moment, the program computes synthetic seismograms. The effect of the free surface is approximately taken into account by multiplying the infinite-space synthetics by a factor of two. This yields approximate half-space synthetics. The accuracy of this approximation can be roughly evaluated from the expressions for total displacement on the free surface of a half-space due to incident plane P and SV waves (Aki and Richards, 1980, vol. 1, p. 190). These expressions show that, for a Poisson solid with β = 3.5 km/s, the error in the amplitude resulting from the approximation is less that 30% for incidence angle i_0 less than about 30^0. Henceforth, we will use the term infinite-space synthetics to mean approximate half-space synthetics. The SV-P conversion beyond the critical angle gives rise to complex SV wave form. This effect is less on the Z component. As mentioned later, the record length used in the inversion excludes SV wave which arrives before the SH wave and is not unipolar. This weaning of the seismograms assures us of the validity of the infinite-space model. Let us denote these corrected synthetic seismograms by u_{1j}, u_{2j}, u_{3j}. The misfit function, $\varepsilon(M_0,\delta,\lambda,\varphi)$ is defined as:

$$\varepsilon(M_0, \delta, \lambda, \varphi) = \sum_{i=1}^{N} \sum_{j=1}^{3} u_{ij} \int_{R_i/\alpha_i}^{T_{ij}} \left(U_{ij}(t) - u_{ij}(t)\right)^2 dt$$

where N is the number of stations, w_{ij} is the weight assigned to component j at station i, Tij is the duration of component j at station i chosen for inversion, and R_i/α_i is the arrival time of P waves to station i.

The inversion algorithm permits different values of α, β, and ρ for different stations. Before starting the inversion, the value β for each source-station path is changed until the S-wave of the synthetic seismogram gets aligned with recorded one. In this selection of β, the synthetics seismograms are calculated for any focal mechanism and the source-time function is prescribed by inspection of the recorded seismograms. The shape of this function may be taken as a triangle or a trapezoid. An arbitrary function may also be chosen. This option allows the source shape to be the same as the recorded body waves. The inversion is performed after the source time function and β for each source-station path is fixed. We note that there is no provision for including directivity effect in the inversion. Also, we do not use a distance-scaling factor to compensate for the amplitude decay with distance as proposed by Zhu and Helmberger (1996). In our case, as the distance increases the infinite-space solution becomes less tenable. This suggests that the farther stations should be given smaller weights. Thus, the amplitude decay with distance automatically provides the desirable effect of smaller weight to data at larger distances.

We note that in the formulation given above, the synthetic seismograms are not corrected for the attenuation. At short distances this effect may not be important, except for very small earthquakes. It is straightforward to modify the algorithm to include the attenuation effect by convolving the synthetics by an appropriate t^* operator.

A grid search is performed over M_0 and focal mechanism parameters φ, δ, and λ to select the set which minimizes the misfit function. The algorithm saves the best five solutions.

Table 1. Crustal structure used in tests with synthetic seismograms

Layer No.	Thickness km	V_P km/s	$V_{]rmS}$ km/s	Q_p	Q_s
1	10.0	5.78	3.35	300	100
2	16.0	6.70	3.85	500	150
3	8.0	7.40	4.27	1000	400
4	–	8.40	4.62	1000	400

Examples

Below we present examples of the application of the inversion technique outlined above. The purpose of

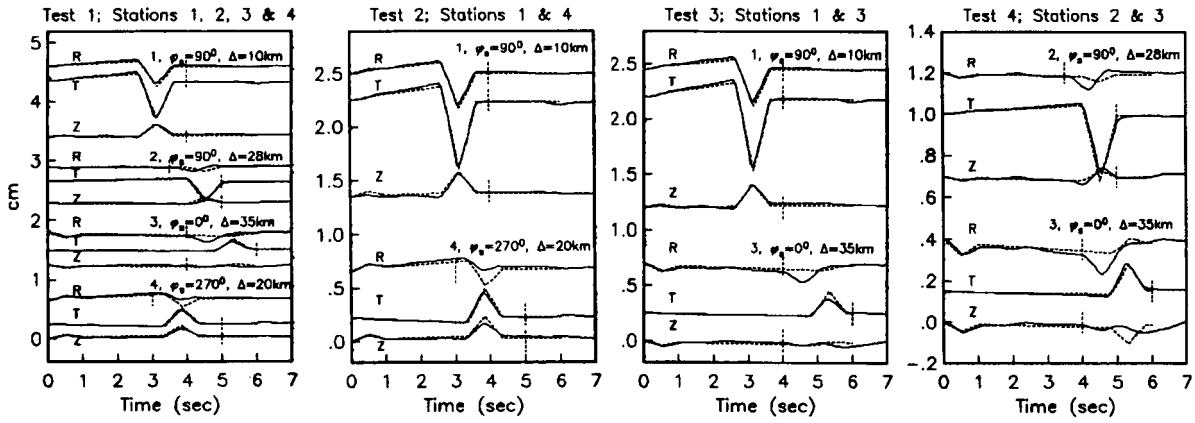

Figure 1. Tests of the inversion technique on synthetic displacement seismograms calculated for a layered, half-space (Table 1), with the source at a depth 16 km, $M_0 = 1 \times 10^{24}$ dyne-cm, and $\varphi = 295^0$, $\delta = 15^0$, $\lambda = 90^0$. Stations whose seismograms are used in each test are indicated. The vertical dotted line shows the record length used in the inversion. R, T, and Z indicate radial, transverse, and vertical components, respectively.

Table 2. Location of stations in the synthetic tests

Station	Epicentral distance Δ, km	Azimuth φ_s
1	10	90^0
2	28	90^0
3	35	0^0
4	20	270^0

these examples is to examine the validity of the technique. We first test the method by inverting synthetic seismograms, calculated for a layered half-space. We then present representative examples of inversion of near-source seismograms of some Mexican earthquakes and two aftershocks of the Umbria-Marche, central Italy earthquake sequence of 1997. In the inversion, a coarse, global grid search is first performed by changing the azimuth, dip, and rake in steps of 10^0. The best five solutions are almost always similar if two or more near-source recordings are available. A fine grid search is then performed over a limited range of fault parameters by changing them in steps of 2.5^0 or less. In all examples given below, except one, the records are shown in cylindrical coordinates centered at the epicenter: the radial component is positive away from the epicenter towards the station, the transverse component is positive 90^0 to the left of the radial direction, and vertical is positive up. We will denote radial, transverse, and vertical directions by R, T, and Z, respectively.

Synthetic cases

We generated synthetic seismograms at four stations using Bouchon's (1982) algorithm The crustal structure is given in Table 1. The stations location are listed in Table 2. In the computation the focal mechanism was taken as $\varphi = 295^0$, $\delta = 15^0$, $\lambda = 90^0$. The point source was located at a depth of 20 km and had a seismic moment $M_0 = 1.0 \times 10^{24}$ dyne-cm. The source time function was taken to be an isosceles triangle with a base of 1.0 s. We present four tests on the synthetic data, which we take as the 'observed' seismograms.

Test 1. In this case the seismograms from all four stations were used in the inversion. Figure 1, left frame, shows the 'observed' seismograms at the four stations (continuous curves) and the length of the record used in the inversion (vertical dashed lines). At each station the seismograms are aligned with the arrival of the P wave. At station 1, the S-wave is simple, unipolar, arrives at the same time, and has the same duration on all the three components. The ramp between P and S waves is the contribution from the near-field terms. These seismograms, although generated for a layered half-space, appear like those expected from a point-source dislocation in an infinite medium. For this reason, the record length chosen for inversion extends until the end of the S-wave and is the same for the three components. At station 2, S-wave on transverse (T) and vertical (Z) components arrives at about the same time, has the same duration, and is unipolar. For this reason, the record length chosen for these two components includes the S wave. The radial

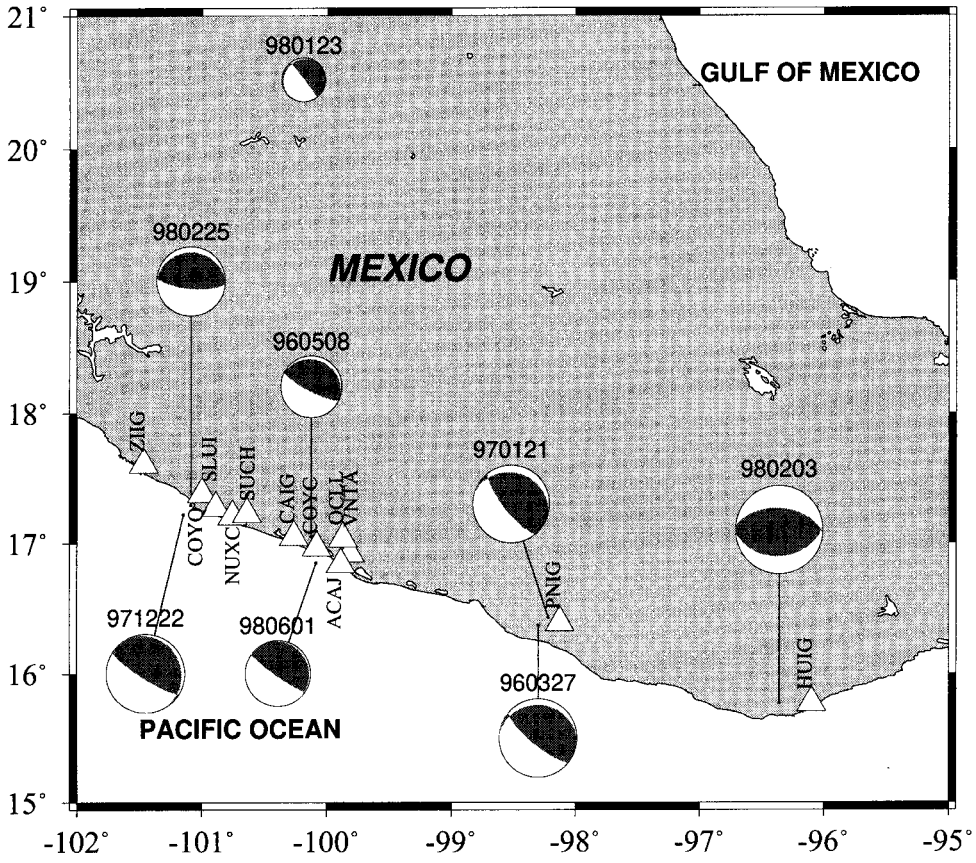

Figure 2. Map showing location and focal mechanism of Mexican earthquakes studied in this paper. The triangles show permanent stations which provided the near-source data.

(R) component shows SP phase arriving before the S wave and the pulse is not unipolar. As the infinite-space model used in the inversion does not include this complication, the record length chosen stops before the arrival of SP phase. Following the same criteria, at station 3 the length of transverse component used in the analysis includes SH wave but stops before S wave on R and Z component. Finally, at station 4 the record length chosen includes S wave for T and Z components but stops before S wave for R component.

The source-time function was taken to be the same as the one used in computing the synthetics. We recall that the program permits selection of P and S wave speeds for each station. This feature allowed an adjustment of these speeds so that the synthetic S wave arrives at the same time as the observed S wave. The coarse, global grid search gave the best solution as $\varphi = 270^0$, $\delta = 20^0$, $\lambda = 70^0$, and $M_0 = 9.0 \times 10^{23}$ dyne-cm. The four next best solutions were similar. A fine grid search was carried out by varying φ from 250^0 to 300^0, δ from 15^0 to 25^0 and λ from 60^0 to 90^0. The best solution was $\varphi = 290^0$, $\delta = 17.5^0$, $\lambda = 85^0$ and $M_0 = 8.5 \times 10^{23}$ dyne-cm. The synthetic waveforms, corresponding to these source parameters, are shown in Figure 1 (left frame) by dashed lines. The fit to the 'observed' seismograms is quite good.

Test 2. In this case we inverted 'observed' seismograms from two of the closest stations, namely 1 (Δ = H/2) and 4 (Δ = H). The seismograms and the record lengths chosen for inversion are shown in Figure 1 (second frame from left). The procedure followed was the same as in the case of Test 1. The inversion gave the best solution as $\varphi = 285^0$, $\delta = 20^0$, $\lambda = 85^0$ and $M_0 = 8.9 \times 10^{23}$ dyne-cm. Again, these source parameters are close to the true ones. The synthetic seismograms, shown by dashed lines in Figure 1 fit well the 'observed' seismograms.

Table 3. Earthquake source parameters

Date	Time	Lat (^{0}N)	Lon (^{0}E)	Depth km	Strike	Dip	Rake	M_0 dyne-cm	Source-time function
96/03/27[a]	12:34	16.37	–98.30	18.0	273^0	18^0	55^0	1.4×10^{24}	Triangle[f] (0.5, 1.0 s)
[b]					291^0	10^0	80^0	1.2×10^{24}	Same as above
[c]					270^0	16^0	66^0	2.1×10^{24}	–
96/05/08[a]	01:24	17.05	–100.13	24.0	292^0	13^0	85^0	2.4×10^{22}	Triangle[f] (0.2, 0.4 s)
97/01/21[a]	21:19	16.43	–98.22	21.0	285^0	20^0	55^0	1.1×10^{24}	See text
[d]					296^0	18^0	70^0	1.2×10^{24}	Complex source
[c]					265^0	18^0	42^0	1.7×10^{24}	–
97/10/07[a]	01:24	43.03	12.84	5.7	165^0	60^0	-28^0	2.3×10^{22}	Triangle[f] (0.25, 0.50 s)
[e]					126^0	26^0	-102^0	2.3×10^{22}	–
97/10/16[a]	12:00	43.04	12.89	3.8	285^0	90^0	178^0	1.3×10^{23}	Triangle[f] (0.30, 0.60 s)
[e]					287^0	80^0	175^0	3.9×10^{22}	–
97/12/22[a]	05:22	17.22	–101.15	20.0	329^0	11^0	116^0	1.4×10^{24}	Triangle[f] (0.8, 1.6 s)
98/01/23[a]	01:23	20.52	–100.19	5.0	322^0	88^0	-100^0	4.4×10^{20}	Triangle[f] (0.1, 0.2 s)
98/02/03[a]	03:02	15.77	–96.36	29.0	274^0	50^0	95^0	1.4×10^{25}	See Figure 5a
[g]					295^0	44^0	108^0	3.5×10^{25}	–
98/02/25[a]	17:09	17.29	–101.09	24.4	270^0	18^0	55^0	1.7×10^{23}	Triangle[f] (0.4, 0.8 s)
98/06/01[a]	07:59	16.85	–100.09	25.7	330^0	7^0	115^0	8.3×10^{22}	Triangle[f] (0.3, 0.7 s)

[a] Focal mechanism, M_0, and source time from this study.
[b] Focal mechanism, M_0, and source-time function obtained by trial and error (Singh et al., 1997).
[c] Focal mechanism and M_0 from inversion of long-period regional waves (Pacheco and Singh, 1998).
[d] Focal mechanism, M_0, and source-time function obtained by trial and error (Pacheco and Singh, 1998).
[e] Focal mechanism and M_0 from Ekström et al. (1998).
[f] For a triangular source, the first number in the parenthesis refers to rise time and the second one to the total pulse duration.
[g] Harvard CMT solution.

Test 3. As in the previous test, we inverted seismograms from only two stations. However, we replace station 4 by station 3, which is located at an epicentral distance of 35 km. Figure 1 (third frame from left) shows the 'observed' and synthetic seismograms and the record length used in the inversion. The inversion gave the best solution as $\varphi = 320^0$, $\delta = 20^0$, $\lambda = 115^0$ and $M_0 = 8.2 \times 10^{23}$ dyne-cm.

Test 4. Records from stations 2 and 3 were used in the inversion. Both stations are located at epicentral distance greater than the depth. Even in this case the inversion gave reasonable solution: $\varphi = 310^0$, $\delta = 10^0$, $\lambda = 110^0$ and $M_0 = 7.5 \times 10^{23}$ dyne-cm.

In the tests above, the inversions yielded focal mechanism solutions which were reasonably close to the true one. The estimated seismic moments were within 75% of the correct value. Clearly, observed displacement seismograms will be more complicated than the synthetic ones used in the tests, both because the crustal structure would be more complicated than a horizontally layered model and because of the noise introduced during integration of velocity or acceleration traces to obtain the displacement seismograms. We are, however, encouraged by the tests. Below we apply the technique to observed seismograms.

Application to recorded data

We illustrate the inversion technique to near-source recordings of some Mexican and a few Italian earthquakes.

(a) Mexican earthquakes

The locations of the earthquakes and permanent stations are shown in Figure 2. The source parameters of the events are listed in Table 3. Stations PNIG, HUIG, ZIIG, and CAIG are permanent broadband stations (Quanterra 24-bit digitizer connected to a Streckeisen STS-2 seismometer and a Kinemetrics FBA-23 accelerometer). Stations, which are identified by a number in the text (not shown in Figure 2), are portable broadband seismographs (RefTek 24-bit digitizer connected to a Guralp CMG40T seismometer). All other stations are equipped with Kinemetrics' K2 (19 bit) or Etna (18 bit) accelerographs. Generally, the displacement

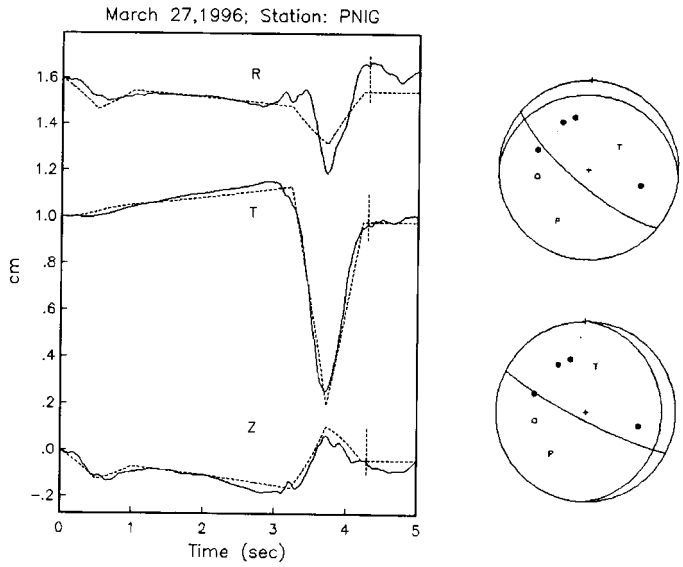

Figure 3. Observed near-source seismograms (continuous curves) of March 27, 1996 Pinotepa Nacional, Mexico, earthquake. Synthetic seismograms (dashed curves) correspond to the focal mechanism and the seismic moment obtained from the inversion. The vertical dashed line indicates the length of the record used in the inversion. The two focal mechanisms (equal-area projection of the lower focal sphere), shown on the right, are equally acceptable solutions from the inversion and the first-motion data.

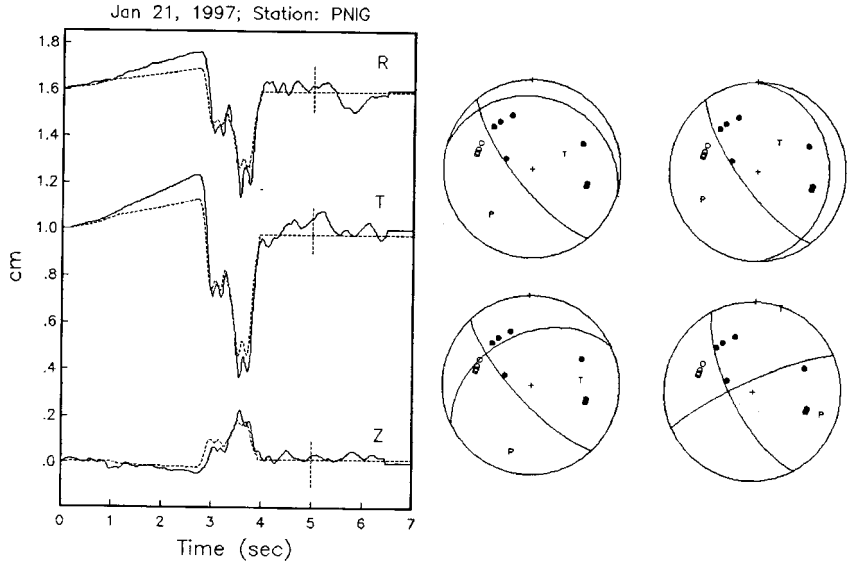

Figure 4. Observed and synthetic seismograms of January 21, 1997 Pinotepa Nacional, Mexico, earthquake. The four focal mechanisms shown in the figure are nearly equally acceptable solutions from the inversion. From the first-motion data, the bottom two focal mechanism may be discarded. The source-time function used in the inversion is the same as the SH pulse on T component.

seismograms obtained from direct integration of velocity records of the broadband seismographs are more reliable than those obtained by double integration of accelerograms. In integrating accelerograms we used a modified version of the technique proposed by Iwan et al. (1985).

Examples of single-station recordings

1. Pinotepa Earthquake of 27 March, 1996. This earthquake was recorded by the permanent broadband station of Pinoptepa Nacional (PNIG). Singh et al. (1997) analyzed the data from this single station to locate the earthquake. The depth of the source (H), the epicentral distance (Δ), and the azimuth of the station (φ_s) were estimated as 18.0 km, 19.7 km, and 82^0, respectively. It should be noted, however, that the event location, the rotation of seismograms in radial and transverse components, and the angle of incidence at the surface, estimated from a single, near-source recording, are subject to error due to the presence of the near-field term. In the previous study, the displacement seismograms were modeled by trial and error, with the help of synthetic seismograms generated for a layered crustal structure appropriate for the region (a layer with α = 5.0 km/s and thickness of 1.5 km overlying a half space with α = 6.2 km/s). In modeling, the range of focal parameters was constrained by the first-motion data. The point source whose synthetics fit the observed data well had the following parameters: seismic moment, $M_0 = 1.2 \times 10^{24}$ dyne-cm; source time function: a triangular pulse of 0.9 sec duration; nodal plane: strike $\phi = 291^0$, dip $\delta = 10^0$, and rake $\lambda = 80^0$. We inverted the displacement seismograms of this event using the technique outlined above. Based on the location given by Singh et al. (1997) we took hypocentral distance R = 26.7 km and $\varphi_s = 82^0$. The source-time function was taken to be the same as in the previous study. Of the five best solutions obtained from the coarse global grid search, two were independent: $\varphi = 270^0$, $\delta = 20^0$, $\lambda = 50^0$, $M_0 = 1.4 \times 10^{24}$ dyne-cm; $\varphi = 110^0$, $\delta = 90^0$, $\lambda = 50^0$, $M_0 = 1.0 \times 10^{24}$ dyne-cm. A fine grid search around the two independent solutions gave the following two source parameters: $\varphi = 272.5^0$, $\delta = 17.5^0$, $\lambda = 55^0$, $M_0 = 1.4 \times 10^{24}$ dyne-cm; $\varphi = 117.5^0$, $\delta = 82.5^0$, $\lambda = 75^0$, $M_0 = 1.2 \times 10^{24}$ dyne-cm. Synthetic seismograms from the two solutions almost equally well fit the observed ones and satisfy the available first-motion data (Figure 3). The first solution is close to the one given by Singh et al. (1997). Without further seismological or tectonic information it is not possible to select the true mechanism.

2. Pinotepa Earthquake of 21 January, 1997. This event, which gave rise to near-source recordings at the broadband station of PNIG, was analyzed by Pacheco and Singh (1998). The depth of the source (H), the epicentral distance (Δ), and the azimuth of the station (φ_s) were estimated as 20.9 km, 10.2 km, and 153.6^0, respectively. The recordings at PNIG were modeled by Pacheco and Singh (1998) by trial and error, with the help of synthetics generated for the same layered crustal structure as the previous case. Two subevents were required to fit the observed seismograms. The trial and error procedure gave the following source parameters: $\varphi = 291^0$, $\delta = 10^0$, and $\lambda = 80^0$; $M_0 = 1.2 \times 10^{24}$ dyne-cm. We inverted the PNIG seismograms using the method developed in this paper. The source time function was taken to have the same shape as the SH pulse (Figure 4). The inversion gave four acceptable solutions; two of these, however, do not fit the first-motion data (Figure 4). The two acceptable solutions are: $\varphi = 285^0$, $\delta = 20^0$, $\lambda = 55^0$, $M_0 = 1.13 \times 10^{24}$ dyne-cm; $\varphi = 359^0$, $\delta = 20^0$, $\lambda = 124^0$, $M_0 = 1.34 \times 10^{24}$ dyne-cm. As in the previous case, synthetic seismograms from the two solutions almost equally well fit the observed ones and satisfy the available first-motion data. The first solution is close to the solution given by Pacheco and Singh (1998).

3. Puerto Angel Earthquake of 3 February, 1998. The Harvard CMT solution of this earthquake is: $\varphi = 295^0$, $\delta = 44^0$, $\lambda = 108^0$, $M_0 = 3.5 \times 10^{25}$ dyne-cm (Mw = 6.4). The earthquake was recorded by the broadband station of HUIG. Since the velocity channel at HUIG was clipped during the S-wave, the displacement seismograms were obtained by direct integration of the acceleration traces. From this recording we estimate H 28 km, $\Delta \sim 28$ km, and $\varphi_s \sim 90^0$. The expected rupture length, L, for this event is 15 to 20 km. For a point-source approximation to be valid, the period of interest should be greater than about 5 s (so that the wavelength $\lambda > L$). An examination of the seismograms (Figure 5) suggests that a point-source is not an adequate approximation of the source. We, nevertheless, inverted the seismograms to investigate if a reasonable solution could be obtained in this adverse condition. In view of the first-motion data (Figure 5a), we limited the grid search to $270^0 \leq \varphi \leq 290^0$, $40^0 \leq \delta \leq 70^0$, $60^0 \leq \lambda \leq 160^0$. We took the shape of the source-time function to be the same as the SV-wave on the Z component (Figure 5a). The best solution

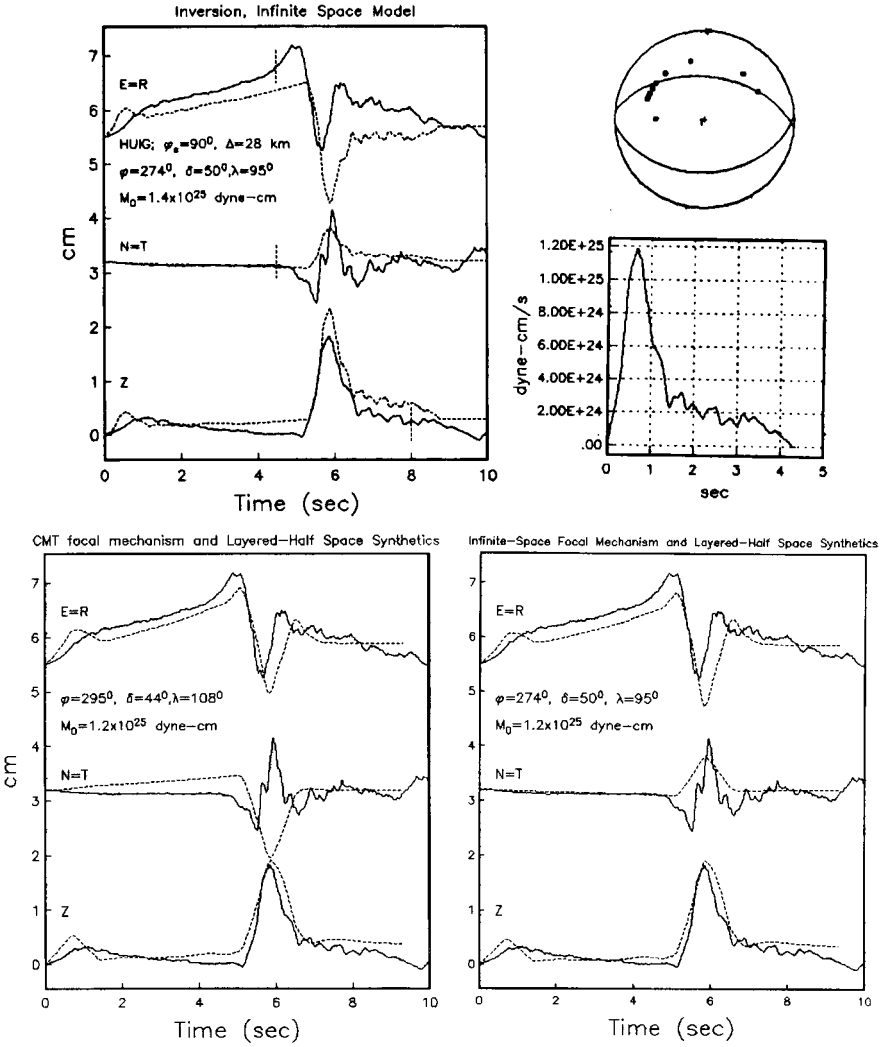

Figure 5. (a) Observed and infinite-space, synthetic seismograms of February 3, 1998 Puerto Angel, Mexico, earthquake. Of the various acceptable solutions, the one which fits the first-motion data is shown on the right. The shape of SVwave on Z component has been taken as the shape of the moment rate function (right, bottom). (b) Left. Comparison of the observed seismograms with synthetic ones computed for a layered half space and the Harvard CMT focal mechanism but with M_0 estimated from local data. Right. Same as the case on the left but with focal mechanism from the inversion of the local data.

from the inversion was: $\varphi = 274^0$, $\delta = 50^0$, $\lambda = 95^0$, $M_0 = 1.4 \times 10^{25}$ dyne-cm. This focal mechanism is similar to the Harvard CMT solution but the seismic moment is only 40% of the CMT value, perhaps reflecting a long-period, slow slip on the fault not resolved by the data. The fit by the synthetics to the observed traces is fair. In Figure 5b we show synthetics seismograms generated for the layered, crustal structure used in the previous two examples. The figure illustrates the synthetics corresponding to the CMT focal mechanism (left) and the focal mechanism obtained from the inversion of the HUIG seismograms. The source-time is an isosceles triangle with a base of 1.8 s. Although the transverse component at HUIG is better fit by our solution than by the CMT solution, the layered, half-space synthetics still poorly fit the observed seismograms, suggesting an inadequate crustal structure. In summary, the analysis of HUIG record indicates that a reasonable solution may be obtained from the inversion even in cases where the point-source approximation is not strictly valid

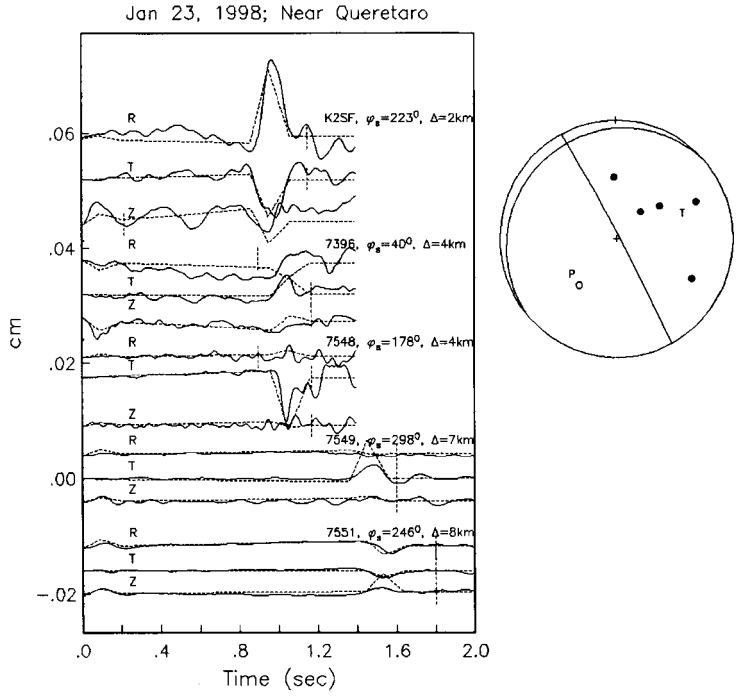

Figure 6. Observed and synthetic seismograms of January 23, 1998 earthquake which occurred near Queretaro, Mexico. The focal mechanism obtained from the inversion is in agreement with the first-motion data and the seismotectonics of the region.

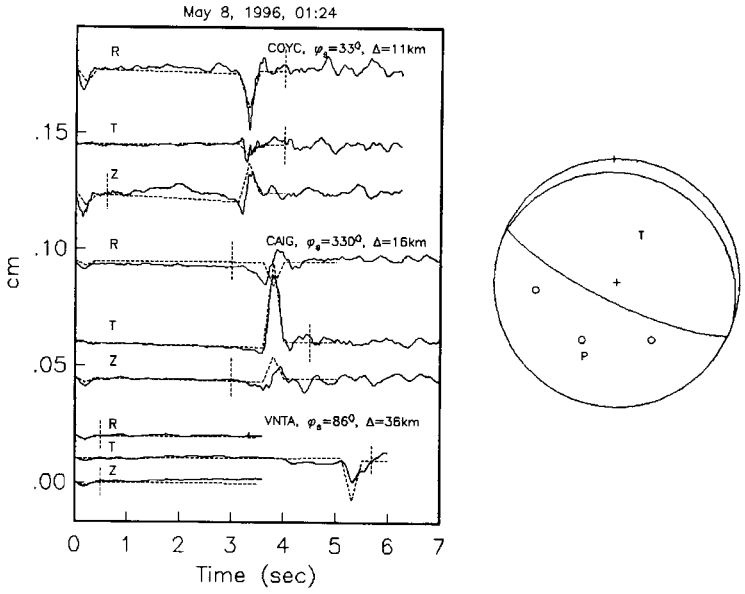

Figure 7. Observed and synthetic seismograms of May 8, 1996 earthquake which occurred NW of Acapulco, Mexico. Shallow, thrust fault plane obtained from the inversion is in agreement with the few first-motion data and the seismotectonics of the region.

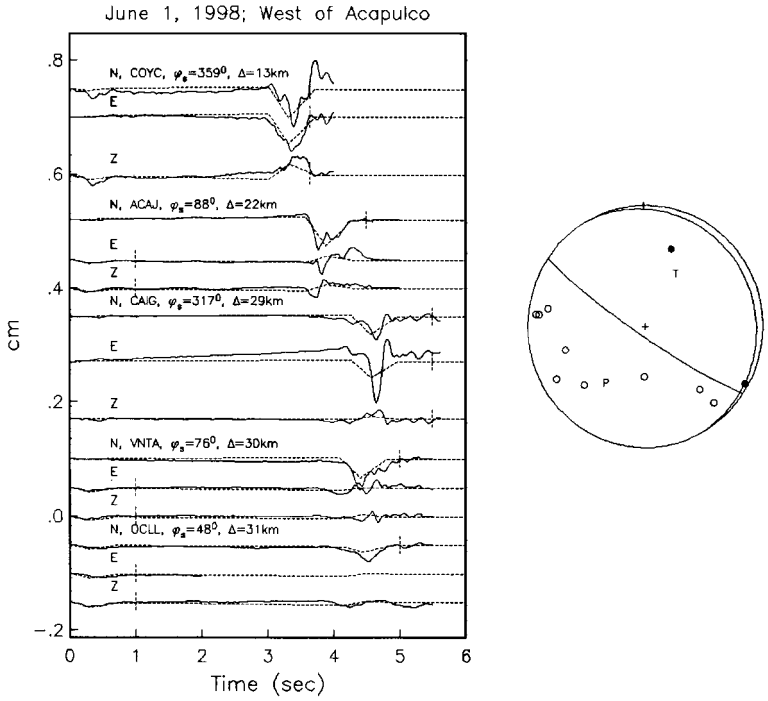

Figure 8. Observed and synthetic seismograms of June 1, 1998 earthquake which occurred W of Acapulco, Mexico. Shallow, thrust fault plane obtained from the inversion is in agreement with the first-motion data and the seismotectonics of the region.

Examples of earthquakes with multiple recordings

As shown above, the tests on synthetic data suggest that we may expect unambiguous solution from the inversion of multiple, near-source recordings. In the following we give several examples of earthquakes with multiple recordings. The magnitude range of the events is $3.1 \leq M_w \leq 5.4$. The epicentral distance to the depth ratios, Δ/H, of the recordings included in the inversion are less than or equal to 1.6, except for the largest earthquake for which $\Delta/H = 2.75$ for one of the recordings. An independent check on the estimated parameters is possible only in few events. In each case, however, the focal mechanism obtained from the inversion agrees with the available first-motion data and known seismotectonics of the region.

Figures 6 to 10 illustrate, in increasing order of M_w, observed and synthetic seismograms of five Mexican earthquakes. These figures give station names, their epicentral distances and azimuths, and indicate the length of the records used in inversion These figures also include lower-hemisphere, equal-area projection of the first-motion data and the focal mechanism obtained from the inversion. The source parameters of the earthquakes are listed in Table 3. We point out that for each of these earthquakes the five best solutions obtained from the inversion were very similar to each other. As seen in Figures 6 to 10, the focal mechanism solutions fit well the first-motion data. These focal mechanisms are consistent with known seismotectonics of the region: shallow thrust along the Mexican subduction zone and N-S normal faulting for the January 23, 1998 earthquake (Figure 2).

We repeated the inversion of these events using seismograms of only two of the nearest stations. The solutions obtained were similar to those listed in Table 3. If the two stations covered an azimuth greater than 90^0 then the solutions were nearly identical.

(b) Umbria-Marche, Central Italy, aftershock sequence of 1997

The Umbria-Marche earthquake sequence began with a foreshock on September 3, 1997 (M_L = 4.7), and was followed by two earthquakes on September 26, 1997 (Mw = 5.7, 6.0). An intense aftershock activity followed which was well recorded by portable seismographs (Amato et al., 1998). The centroid moment tensors of fourteen of the larger events (Mw>4.2) of the entire sequence was obtained by Ekström et al.

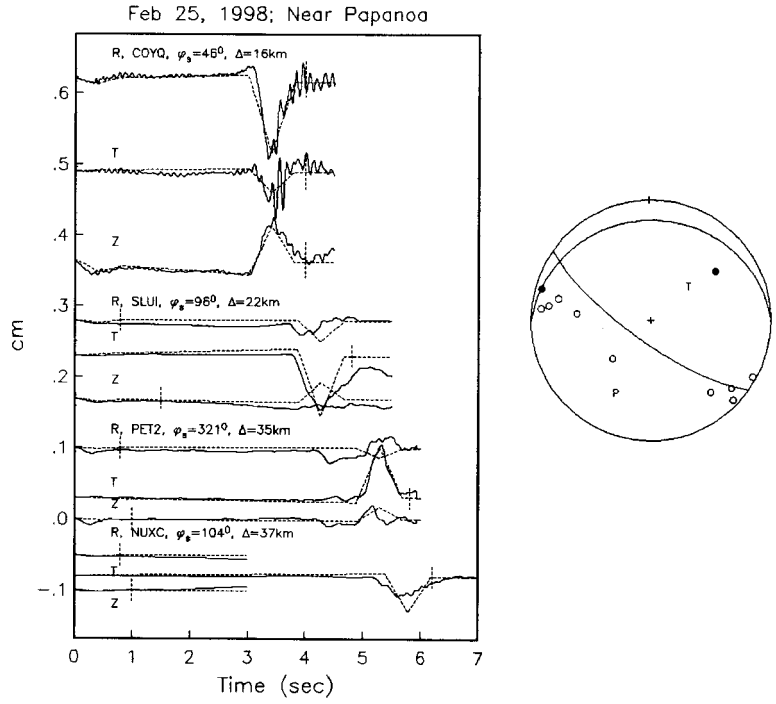

Figure 9. Observed and synthetic seismograms of February 25, 1998 earthquake which occurred near Papanoa, State of Guerrero, Mexico. Shallow, thrust fault plane obtained from the inversion is in agreement with the first-motion data and the seismotectonics of the region.

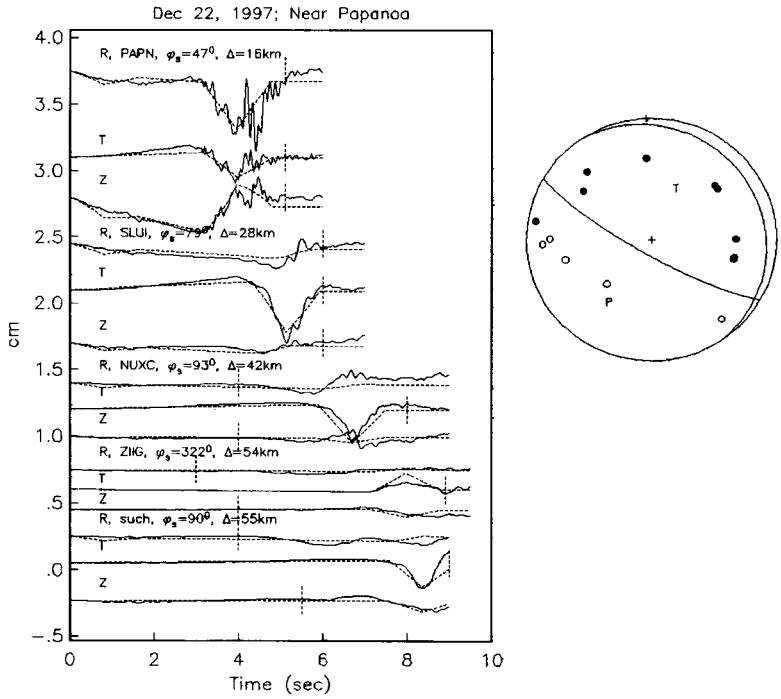

Figure 10. Observed and synthetic seismograms of December 22, 1998 earthquake which occurred near Papanoa, State of Guerrero, Mexico. Shallow, thrust fault plane obtained from the inversion is in agreement with the first-motion data and the seismotectonics of the region.

Table 4. Crustal structure used in locating Umbria-Marche aftershocks and in generating synthetic seismograms

Layer No.	Thickness km	V_P km/s	V_S km/s	Q_p	Q_s
1	4.0	4.8	2.77	300	100
2	3.0	5.5	3.18	500	150
3	23.0	6.3	3.64	1000	400
4	–	8.0	4.62	1000	400

(1998), who analyzed regional, long-period surface waves by applying a modified version of the Harvard CMT algorithm. We applied our inversion scheme to the local data of some of the events analyzed by Ekström et al. Because of shallow depth of the aftershocks ($\sim$ 5 km) and site effects, these events provide an extreme test of the proposed technique. We found that our results were, generally, very similar to those reported by Ekström et al. (1998). Below we present analysis of two of these events which illustrates the robustness as well as limitations of the method.

October 7, 1997 (01:24) aftershock.
When we began analysis of this event, the only on-scale, near-source recordings available to us were accelerograms from two stations: ANNI and COLF (Figure 11). In the analysis we took the source-time function as an isosceles triangle with a base of 0.4 s. The inversion yielded the following source parameters: $\varphi = 165^0$, $\delta = 60^0$, $\lambda = -28^0$, and $M_0 = 2.3 \times 10^{22}$ dyne-cm. Additional seismograms from two more stations (PENN and COST) in the inversion only slightly modified the solution: $\varphi = 163^0$, $\delta = 60^0$, $\lambda = -33^0$, and $M_0 = 1.9 \times 10^{22}$ dyne-cm. The source parameters given by Ekström et al. (1998) are: $\varphi = 126^0$, $\delta = 26^0$, $\lambda = -102^0$, and $M_0 = 2.3 \times 10^{22}$ dyne-cm. While the seismic moments from the two inversions are about equal, the focal mechanisms are significantly different. Figures 11a and 11b illustrate observed and synthetic seismograms corresponding to the two source parameters. The fit is poor in both cases but is much worse for the source parameters reported by Ekström et al. (see the transverse components at ANNI and COLF, Figure 11b). These figures also show the first-motion data. The focal mechanism obtained from the inversion of the local data is in better agreement with the first-motion data. We conclude that the focal mechanism of this event obtained from the inversion of the local data is more reliable that the one obtained from CMT inversion of regional seismograms. Figure 12 shows synthetics computed for the crustal structure used in the location of Umbria-Marche earthquake sequence (Table 4) and compares these synthetics with the observed seismograms. The synthetics shown in the left- and the right-hand side of the figure correspond to the source parameters obtained from this study and by Ekström et al. (1998), respectively. Again the fit is better with the solution obtained in this study. More importantly, from inspection of the waveforms on the left-hand side it seems that essentially the same focal mechanism (although a higher value of M_0) would have been obtained by inverting the seismograms using layered half-space synthetics.

October 16, 1997 aftershock.
This aftershock provides an extreme test of our inversion scheme. This is the only strike-slip event listed by Ekström et al. (1998); all others are normal-faulting earthquakes. Since the depth of the event is only 3.8 km, the seismograms are expected to be complicated and dominated by surface waves. We inverted on-scale, near-source recordings from stations COLF and ANNI (Figure 13). The variation of the duration of S-pulses seen in the seismograms in Figure 11 suggests directivity towards the south. Since it is difficult to choose a source-time function, we experimented with a suite of them. Although the synthetics fitted the observed seismograms very poorly in all cases the focal mechanism was, surprisingly, stable and very similar to the one reported by Ekström et al. (1998). Figure 12 illustrates observed and synthetic seismograms corresponding to the best solution obtained from the inversion, assuming an isosceles triangle of 0.6 s base as the source-time function: $\varphi = 285^0$, $\delta = 80^0$, $\lambda = 179^0$, and $M_0 = 1.3 \times 10^{23}$ dyne-cm. As can be seen from the figure, the fit is very poor. The source parameters given by Ekström et al. are: $\varphi = 287^0$, $\delta = 80^0$, $\lambda = 175^0$, and $M_0 = 3.9 \times 10^{22}$ dyne-cm. Both focal mechanisms fit the first-motion data (Figure 13). Note, however, that our inversion yields a seismic moment about three times larger than the one reported by Ekström et al. The seismic moment of this event was estimated by Mazza et al. (1997) from the spectra of S-waves, recorded on two regional broadband seismographs. The median seismic moment reported by these authors, 2.3×10^{23} dyne-cm, is almost 6 times greater than the value found by Ekström et al. and is within a factor of two of the value obtained here.

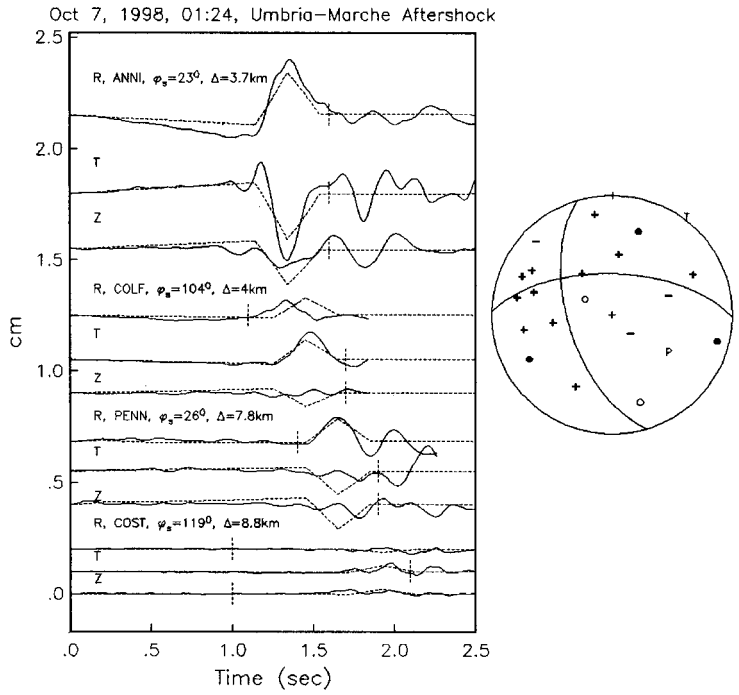

Figure 11. (a). Observed and synthetic seismograms of October 7, 1997 (01:24) Umbria-Marche aftershock. The focal mechanism obtained from the inversion fits the first-motion data well. Solid dot: clear compression; open circle: clear dilatation; plus: emergent compression; minus: emergent dilatation.

Conclusion

The examples above confirm what one would have intuitively expected: simple infinite-space, point-source shear dislocation model of an earthquake may be sufficient to obtain accurate focal mechanism and seismic moment of small and moderate earthquakes from the inversion of near-source, high-quality seismograms. A great advantage of the inversion scheme is its simplicity and speed. Generally, for the recordings to be useful the epicentral distance of the station should be less than the depth of the source. However, recordings at greater epicentral distance may also be used, especially the SH pulse. Inversion of the data from a single station leads to more than one equally acceptable focal mechanisms. The inversion of recorded data in Mexico and Italy, however, yields surprisingly stable and reliable source parameters if the seismograms are available from more than one station. In the examples considered above, the focal mechanism obtained from the inversion of two or more recordings is almost always in good agreement with the first-motion data and, if available, with the source parameters obtained from analysis of regional seismic waves. The inversion scheme implemented in this paper provides a useful tool for interpreting near-source seismograms.

Acknowledgements

We thank our colleagues from Italy and France for facilitating us the aftershock data. Discussions with M. Cocco, T. Mikumo, A. Rovelli, and A. Zollo were very useful to us. The National Seismological Service of Mexico (which is part of Instituto de Geofísica, UNAM) operates the broadband seismic network. The Guerrero Accelerograph Array is a joint project of Instituto de Ingeniería, UNAM and University of Nevada, Reno. We thank the technicians who maintain these two networks often under very adverse conditions. A PC version of the inversion algorithm, which requires Window 95, is available on request from mos@merlin.iingen.unam.mx. The research was partially supported by a European Union project (Contract CI1∗-CT92-0025, DGAPA (UNAM) project IN109598, and CONACYT project 25403-A.

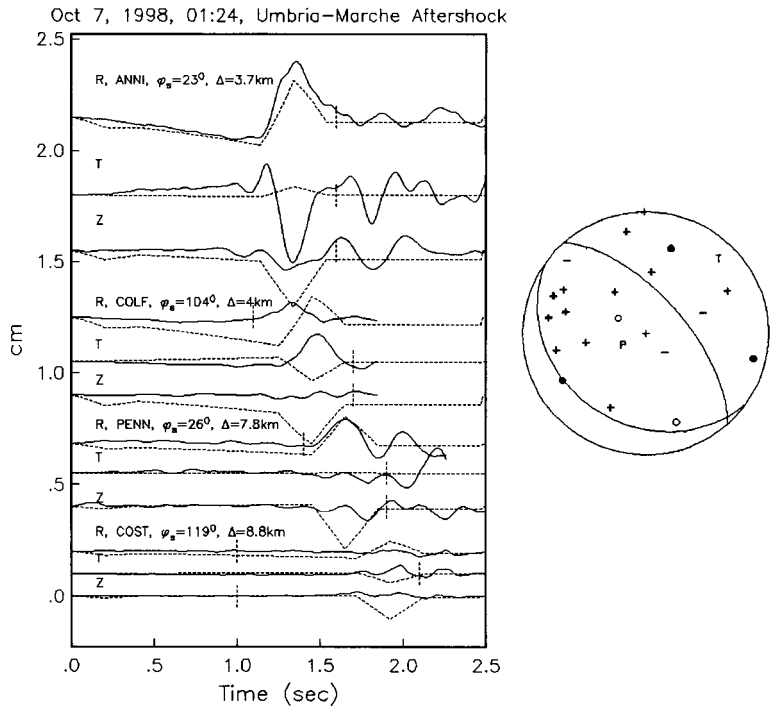

Figure 11. (b) Same as (a) but for the focal mechanism reported by Ekström et al. (1998). Synthetic seismograms corresponding to this focal mechanism provides a poorer fit to observed seismograms and the first-motion data.

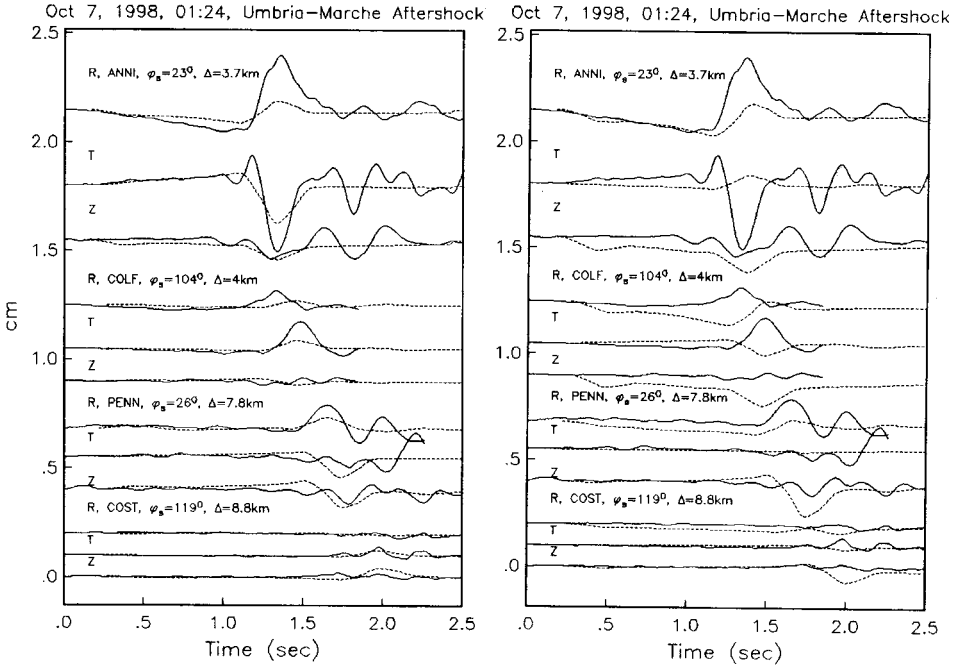

Figure 12. Observed and synthetic seismograms computed of October 7, 1997 1997 (01:24) Umbria-Marche aftershock. Synthetics were computed for a layered crustal model (Table 4). Left: focal mechanism and M_0 form inversion of local data. Right: focal mechanism and M_0 from Ekström et al. (1998).

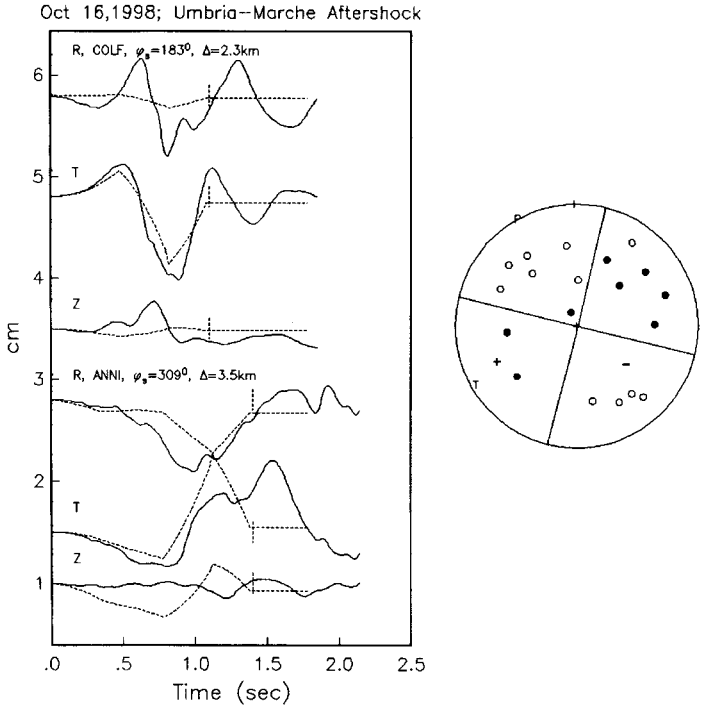

Figure 13. Observed and synthetic seismograms of October 16, 1997 Umbria-Marche aftershock. Although the synthetics fit observed seismograms very poorly, the focal mechanism obtained from the inversion fits well the first-motion data (right).

References

Aki, K., 1968, Seismic displacement near a fault, *J. Geophys. Res.* **73**, 5359–5376.

Aki, K. and Richards, P.G., 1980, *Quantitative Seismology, Theory and Methods*, Vol. I & II, W.H. Freeman and Company, San Francisco.

Amato, A., Azzara, R., Chiarabba, C., Cimini, G.B., Cocco, M., Di Bona, M., Margheriti, L., Mazza, S., Mele, F., Salvaggi, G., Basili, A., Boschi, E., Courboulex, F., Deschamps, A., Gaffet, S., Bittarelli, G., Chiaraluce, L., Piccinini, D. and Ripepe, M., 1998, The 1997 Umbria-Marche, Italy, earthquake sequence: a first look at the main shocks and aftershocks, *Geophys. Res. Lett.* **25**, 2861–2864.

Anderson, J.G. and Richards, P.G., 1975, Comparison of strong ground motion from several dislocation models, *Geophys. J. Roy. Astr. Soc.* **42**, 347–373.

Ben-Menahem, A. and Singh, S.J., 1981, *Seismic Waves and Sources*, Springer-Verlag, New York.

Bouchon, M., 1982, The complete synthetics of crustal seismic phases at regional distances, *J. Geophys. Res.* **87**, 1735–1741.

Ekström, G., Morelli, A., Booschi, E. and Dziewonki, A.M., 1998, Moment tensor analysis of the central Italy earthquake sequence of September-October 1997, *Geophys. Res. Lett.* **25**, 1971–1974.

Iwan, W.D., Moser, M.A. and Peng, C.Y., 1985, Some observations on strong-motion earthquake measurement using a digital acclerograph, *Bull. Seism. Soc. Am.* **75**, 1225–1246.

Jiao, W., Wallace, T.C., Beck, S.L., Silver, P.G. and Zandt, G., 1995, Evidence for static displacement from the June 9, 1994 deep Bolivian earthquake, *Geophys. Res. Lett.* **22**, 2285–2288.

Kanamori, H., Mori, J. and Heaton, T.H., 1990, The 3 December 1988, Pasadena earthquake (M_L = 4.9) recorded with the very broadband system in Pasadena, *Bull. Seism. Soc. Am.* **80**, 483–487.

Love, A.E.H., 1944, *A Treatise on the Mathematical Theory of Elasticity,* Dover Publications, N.Y., 641 p.

Ma, K.-F. and Kanamori, H., 1991, Aftershock sequence of the 3 December 1988 Pasadena earthquake, *Bull. Seism. Soc. Am.* **81**, 2310–2319.

Ma, K.-F. and Kanamori, H., 1994, Broadband waveform observation of the 28 June 1991 Sierra Madre earthquake sequence, *Bull. Seism. Soc. Am.* **84**, 1725–1738.

Mazza, S., Ekström, G. and Piromallo, C., 1997, Magnitudo e momenti scalari, In: Boschi, E. and Cocco, M. (eds), *Studi preliminary sulla sequenza sismica dell'Appenino Umbro-Marchigiano del settembre-ottobre 1997* Istituto Nazionale de Geofisica, Rome, Publ. No. 593, 10–14.

Pacheco, J.F. and Singh, S.K., 1998, Source parameters of two moderate Mexican earthquakes estimated from a single-station, near-source recording, and from MT inversion of regional data: a comparison of results, *Geofísica Internacional* **37**, 95–102.

Romanowicz, B., Dreger, D., Pasyanos, M. and Uhrhammer, R., 1993, Monitoring of strain release in central and northern California, *Geophys. Res. Lett.* **20**, 1643–1646.

Scrivner, C.W. and Helmberger, D.V., 1995, Preliminary work on an early warning and rapid response program for moderate earthquakes, *Bull. Seism. Soc. Am.* **85**, 1257–1265.

Singh, S.K., Pacheco, J.F., Courboulex, F. and Novelo, D., 1997, Source parameters of the Pinotepa Nacional, Mexico, earth-

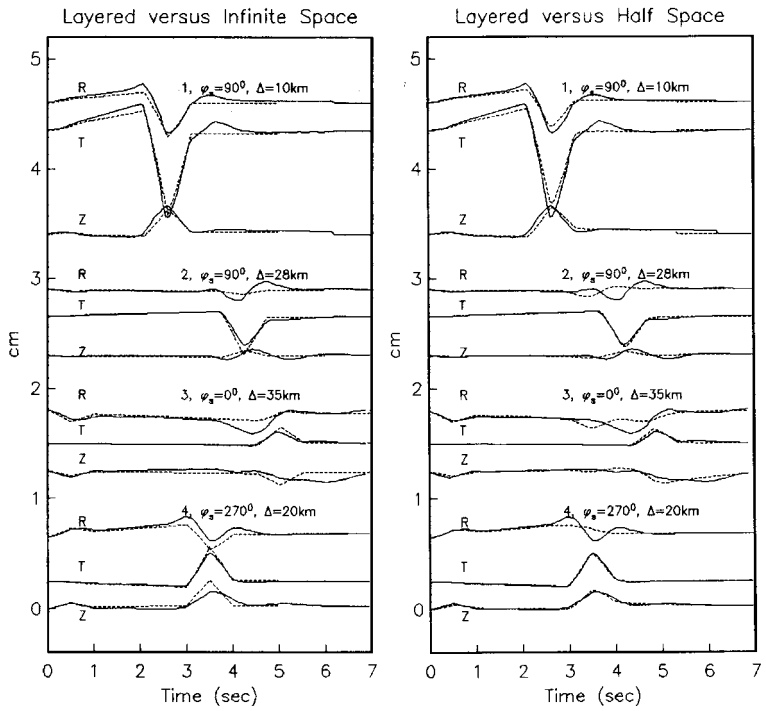

Figure A. A. Left: Synthetic seismograms in a layered crust (continuous line) and in an infinite space (dashed curve). Right: Synthetic seismograms in a layered crust (continuous curve) and in a half space (dashed curve). See appendix for details of the crustal structure. Source depth = 16 km; $M_0 = 1 \times 10^{24}$ dyne-cm; focal mechanism: $\varphi = 290^0$, $\delta = 15^0$, $\lambda = 90^0$; source time function: isosceles triangle with a base of 1 s. The station locations are given in Table 2.

quake of 27 March, 1996 (Mw = 5.4) estimated from near-field recordings of a single station, *J. Seism.* **1**, 39–45.

Stokes, G.G., 1849, Dynamic theory of diffraction, *Cambridge Phil. Soc. Trans.* **9**, 1.

Uhrhammer, R., 1992, Broadband near-field moment tensor inversion, *EOS Trans. A.G.U.* **73**.

Vidale, J.E., Goes, S. and Richards, P.G., 1995, Near-field deformation seen on distant broadband seismograms, *Geophys. Res. Lett.* **22**, 1–4.

Wu, R.-S. and Ben-Menahem, A., 1985, The elastodynamic near field, *Geophys. J. R. Astr. Soc.* **81**, 609–621.

Zhu, L. and Helmberger, D.V., 1996, Advancement in source estimation techniques using broadband regional seismograms, *Bull. Seism. Soc. Am.* **86**, 1634–1641.

Appendix

Here we consider two strategies for the inversion of near-source seismograms: (a) Include SV waves on R and Z components whether or not they are unipolar pulses and use exact half-space synthetics in the inversion. (b) Exclude nonunipolar SV pulses and use approximate half-space synthetics (i.e., infinite–space synthetics multiplied by two).

Let our 'observed' records be synthetic seismograms generated for an earthquake of $M_0 = 1 \times 10^{24}$ dyne-cm, with focal mechanism $\varphi = 290^0$, $\delta = 15^0$, $\lambda = 90^0$, and an isosceles triangular source time function of 1 s duration. Let the source be located at a depth of 16 km in a crustal structure which consists of a layer (α = 4.5 km/s, β = 2.6 km/s, ρ = 2.8 gm/cm^3, Q_α = 300, Q_β = 100, H = 1.5 km) overlying a half space (α = 6.4 km/s, β = 3.7 km/s, ρ = 2.9 gm/cm^3, Q_α = 500, Q_β = 150). In Figure A, these 'observed' records are compared with synthetic seismograms generated for a half space (left) and for an infinite space (right). The station locations are the same as in Table 2. At station 1, located at Δ = 10 km, both infinite- and half-space synthetics are close to the 'observed' records. At station 2 (Δ = 20 km), Z and T half-space synthetics better approximate the 'observed' records than those generated in an infinite space. However, in this example, the infinite-space synthetic for SV-wave on R component is closer to the 'observed' seismogram than the half-space synthetic. At farther stations 2 and 3, infinite- and half-space T-component synthetics provide equally good approximation to the

'observed' data. At these distances, the synthetics for SV wave on R and Z components deviate significantly from the 'observed' records; surprisingly, however, the infinite-space model provides a smaller misfit (see R components at stations 2 and 3 in Figure A). [We note that T components of half-space and infinite-space synthetics in Figure A should exactly be the same. The slight difference seen in the figure comes from the fact that Q is included in the former model but is infinite for the latter model].

In strategy (a) above, one would include SV on all R and Z components and half-space synthetics. Since at some stations these synthetics deviate significantly from the 'observed' seismograms (Figure A, right), the inversion is likely to yield an unreliable result. In strategy (b) above, SV on R component at stations 2, 3, and 4 as well as on Z component at stations 2 and 3 would be excluded from the inversion since they do not arrive at the same time as SH waves and they are not unipolar pulses. We expect this weaning of the seismograms to lead to a reasonably accurate solution. (For the present case, we obtained $M_0 = 1.02 \times 10^{24}$ dyne-cm and $\varphi = 310^0$, $\delta = 17^0$, $\lambda = 110^0$).

The example above is not an extreme case. For real data, there is no simple way to know if half-space is a reasonable model to explain the nonuniploar observed SV waves on R and Z components. Rather than blindly trust the half-space modeling, it may be better to ignore these complex SV waves and use the simple infinite-space model in the inversion. Of course, one may also exclude nonunipolar SV pulses while using half-space synthetics in the inversion, but then it essentially becomes the infinite-space case.